Magnetization and electrical-transport investigation of the dense Kondo system $CeAgSb_2$

E. Jobiliong, J. S. Brooks, and E. S. Choi
Department of Physics/NHMFL, Florida State University, Tallahassee, Florida 32306, USA

H. Lee and Z. Fisk
Department of Physics, University of California at Davis, California 95616, USA

(Received 14 May 2005; revised manuscript received 3 August 2005; published 21 September 2005)

Of the dense Kondo materials in the class $CeTSb_2$ (where T=Au, Ag, Ni, Cu, or Pd), $CeAgSb_2$ is special due to its complex magnetic ground state, which exhibits both ferromagnetic and antiferromagnetic character below an ordering temperature $T_O \sim 9.8$ K. To further elucidate a description of this magnetic ground state, we have carried out a systematic study of single crystalline $CeAgSb_2$ by magnetic, electrical magneto-transport, and Shubnikov-de Haas (SdH) studies. We have constructed the magnetic phase diagram based solely on magnetoresistance data. Here, depending on the orientation of the magnetic field H, either ferromagnetic or antiferromagnetic ordering occurs below T_O. At zero field the temperature-dependent resistivity below T_O is most consistent with antiferromagnetic order, based on the transport theory which includes magnon scattering. The crystal-field-effect theory applied to the susceptibility data yields splitting energies from the ground state to the first and second excited states of 53 K and 137 K, respectively. Based on different models to determine the Kondo temperature T_K, we can obtain both low-temperature and high-temperature estimates for T_K of ~23 K and ~65 K, respectively. In the Fermi surface studies, the measurements show very small Fermi surface sections, not predicted by band-structure calculations, and the SdH amplitudes are very sensitive to field direction.

DOI: 10.1103/PhysRevB.72.104428 PACS number(s): 75.30.Mb, 71.20.Eh, 72.10.Di, 71.70.Ch

I. INTRODUCTION

Cerium intermetallic compounds exhibit a variety of phenomena such as heavy fermion, superconducting, Kondo insulating, anisotropic transport, and magnetic ordering behavior.[1–6] Of current interest in this class of materials are Ce compounds in the tetragonal $ZrCuSi_2$ structure (P4/nmm) including $CeCuAs_2$ and $CeTSb_2$ (where T=Au, Ag, Ni, Cu, or Pd). These compounds exhibit competition between the Ruderman-Kittel-Kasuya-Yosida (RKKY) interaction and the Kondo effect, which leads to either magnetic or nonmagnetic ground states depending on the strength of the magnetic exchange interaction J_{cf} between the conduction electrons and localized 4f spins.[7] For instance, Sengupta *et al.*[8] found non-Fermi liquidlike behavior at a low temperature in $CeCuAs_2$, where the resistivity shows $T^{0.6}$ dependence and no long-range magnetic order is observed.[9] Besides the RKKY interaction and Kondo effect, the crystalline electric field (CEF) also plays a significant role in determining their magnetic properties. The CEF analysis provides important information about the hybridization effect. In addition, as proposed by Levy and Zhang, the CEF potential depends on the hybridization between the conduction band states and the localized f-electron states, which is responsible for the heavy fermion behavior.[10]

Of particular interest is $CeAgSb_2$, following the report of weak ferromagnetic order in polycrystalline samples by Sologub *et al.*[11] On the basis of magnetization studies, it was shown[11] that this compound exhibits a transition below 12 K with a net ferromagnetic moment of $0.15\mu_B$/Ce at 5 K. The crystal structure of $CeAgSb_2$ consists of Sb-CeSb-Ag-CeSb-Sb layers along [001] with lattice constants a=4.363 Å and c=10.699 Å, as shown in Fig. 1.[3,12] Several different groups have investigated the magnetic properties of $CeAgSb_2$ with conflicting results for the interpretation of the magnetic ground state.[6,7,13–16] For instance, Muro *et al.*[6] suggested a ferrimagnetic ground state in polycrystalline samples with a spin-flip field of about 1.3 T. However, this result disagrees with muon spin rotation (μSR) measurements where spectra in both the ordered state and paramagnetic state indicate a single crystallographic and magnetic muon site.[16] Nevertheless, in accordance with μSR measurements,[16] it is very difficult in polycrystalline samples to differentiate between a simple ferromagnetic structure and

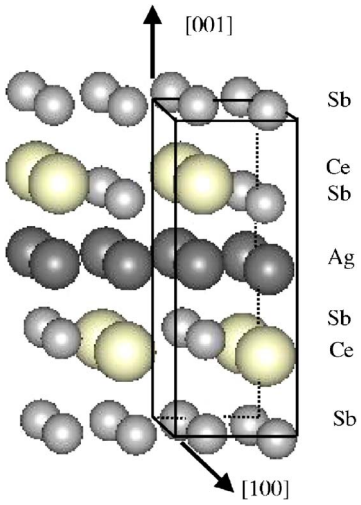

FIG. 1. (Color online) Crystal structure of $CeAgSb_2$. The tetragonal volume defines the unit cell.

a complex antiferromagnetic structure with a resultant ferromagnetic component. Neutron-powder diffraction measurements indicate that the magnetic moment is oriented along the *c* axis with a Curie temperature of about 9.5 K, but with a smaller saturation moment of $\sim 0.4\mu_B$/Ce.[17,18] Inelastic neutron scattering[13] and μSR experiments[16] indicate relatively high Kondo temperatures of 60 to 80 K and 60 K, respectively. However, the magnetic entropy reaches[3] almost $R \ln 2/(\text{mol Ce})$ at the ordering temperature T_O, suggesting that the Kondo temperature is less than T_O, based on entropy arguments.[19] Complex features indicating anisotropy are also evident in electronic transport measurements.

Recent measurements of the de Haas-van Alphen (dHvA) effect[5] have been used to study the Fermi surface of this compound. The electronic specific heat coefficient γ of single-crystal[20] $CeAgSb_2$ is 65 mJ K^{-2} mol^{-1} (75 mJ K^{-2} mol^{-1} for polycrystalline samples[6]) indicative of heavy mass carriers. Effective cyclotron masses from dHvA measurements for fields along the *c* axis are between $0.85m_e$ (m_e is free electron mass) and $32m_e$, for dHvA frequencies between 41 T and 11.2 kT.[5] The band-structure calculations predict that the Fermi surface of $CeAgSb_2$ has a large dHvA frequency of 10.7 kT and several branches with the dHvA frequencies between 4 kT and 9 kT.[5] Only one previous Shubnikov-de Haas (SdH) measurement has been reported for magnetic field parallel to the *c* axis. Here, a single orbit of ~25 T has been observed at 1.2 kbar in the range 18 T at 2.1 K.[21]

The purpose of the present work is to investigate in more detail some aspects of single-crystal $CeAgSb_2$ samples to clarify the assignment of a magnetic ordering in the ground state and to further explore the behavior of the Fermi surface through the quantum oscillations. In particular, detailed studies of the temperature-dependent magnetoresistance can be described by terms involving scattering due to magnons in addition to simple Fermi liquid behavior ($\rho \sim T^2$). This leads to a description of an anisotropic magnetic ground state. Here, ferromagnetic and antiferromagnetic order depends on magnetic field direction. We find that the magnetization and susceptibility are well described by CEF theory where the energy level parameters are consistent with inelastic-neutron-scattering experiments. In addition, we find, as in a previous report, that one quantum oscillation dominates the SdH spectrum, which is smaller in extremal area than any oscillation seen in the previous dHvA study. Angular-dependent SdH studies further reveal unusual aspects of the Fermi surface of this compound.

II. EXPERIMENTS

Single crystals of $CeAgSb_2$ were made with excess Sb as a flux. The starting materials were placed in an alumina crucible and sealed under vacuum in a quartz ampule, heated to 1150 °C, and then cooled slowly to 670 °C and centrifuged to remove the flux. The dc resistivity data were measured using a conventional four-probe method with current applied in the *ab* plane. The typical size of a single crystal is 2.5 mm × 1 mm × 0.3 mm.

The magnetization studies were carried out in a superconducting quantum interference device (SQUID) magnetometer

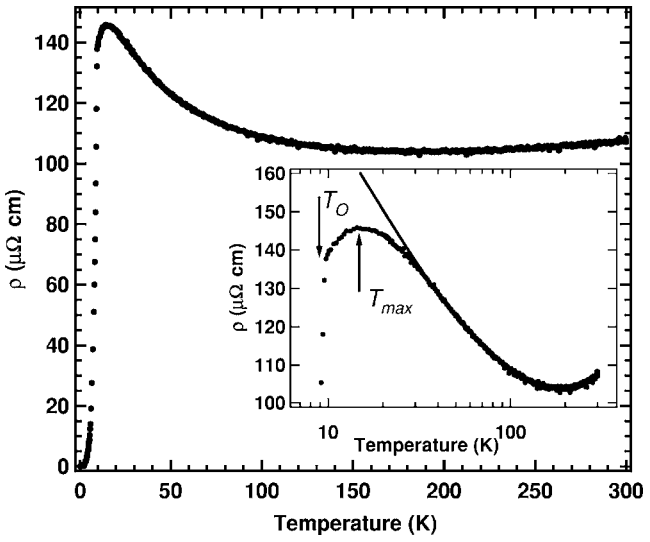

FIG. 2. Temperature dependence of the in-plane dc resistivity of a single crystal of $CeAgSb_2$ between room temperature and ~300 mK. Inset: high-temperature fit (solid line) to Eq. (1).

over the temperature range 1.8–300 K in the field range 0–5.5 T. Shubnikov-de Haas measurements were performed in both a 33 T resistive magnet in a helium-4 cryostat and separately in a 18 T superconducting magnet with a dilution refrigerator.

III. RESULTS AND ANALYSIS

A. Electrical transport properties

The dc resistivity of a single crystal of $CeAgSb_2$ vs temperature in the range room temperature to ~300 mK is shown in Fig. 2. At high temperatures the scattering is phonon dominated and the resistivity decreases with decreasing temperature. However, below ~150 K, the resistivity increases logarithmically as the temperature decreases, which is characteristic of a Kondo lattice system. Below ~15 K, the resistivity exhibits behavior marked by a drop in resistivity as denoted by T_{max} (see the inset of Fig. 2). In the system, where there is magnetic ordering in the Kondo lattice, the value of T_{max} has to be considered as a function of both Kondo temperature and the mean RKKY interaction strength.[22] We are able to fit the temperature dependence of the resisitivity in the range ~300 K– ~30 K, as shown in the inset of Fig. 2, by using[23]

$$\rho(T) = \rho_0^{\infty} - C_1 \ln T + C_2 T^5 \int_0^{\Theta_D/T} \frac{x^5}{(e^x - 1)(1 - e^x)} dx, \quad (1)$$

where ρ_0^{∞} is the resistivity due to spin disorder, C_1 is the Kondo coefficient, C_2 is a temperature-independent constant related to the electron-phonon interaction strength, and Θ_D is the Debye temperature. The second and third terms of Eq. (1) describe the characteristic single-ion Kondo effect and the electron-phonon scattering, also known as the Bloch-Grüneisen relation,

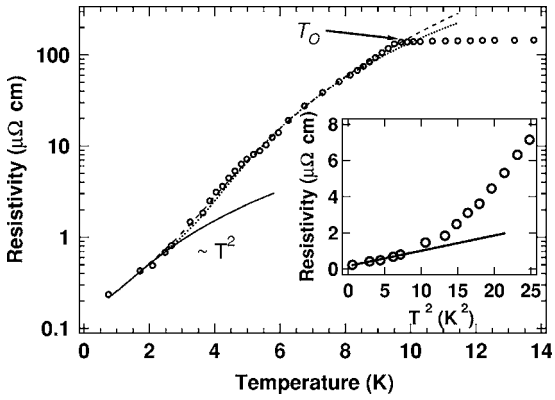

FIG. 3. Temperature dependence of the in-plane dc resistivity of a single crystal of $CeAgSb_2$ at a low temperature. The solid line indicates T^2 dependence and the dashed and dotted line indicate the full fit to Eq. (3) for AFM and FM, respectively. Inset: low-temperature fit of $\rho=\rho_0+AT^2$.

respectively. We find the parameters corresponding to this fit are $\rho_0^{\infty}=(251\pm0.4)$ $\mu\Omega$ cm, $C_1=(33.8\pm0.2)$ $\mu\Omega$ cm, $C_2=(3.08\pm0.02)\times10^{-10}$ $\mu\Omega$ cm K^{-5}, $\Theta_D=(216\pm6)$ K. For comparison, Θ_D is ~200 K for nonmagnetic $LaAgSb_2$, estimated from specific heat measurements.[6,7] Below ~10 K (inset of Fig. 2), the resistivity decreases significantly, corresponding to a magnetic transition at $T_O\sim9.8$ K. The residual resistivity $\rho_0(T\sim300$ mK) and the residual resistivity ratio (RRR) $(=\rho_{room\text{-}temp}/\rho_0)$ are 0.126 $\mu\Omega$ cm and 853, respectively, reflecting a high-quality sample. The temperature dependence of the in-plane dc resistivity below T_O does not follow a simple Fermi-liquid behavior $(\rho\sim\rho_0+AT^2)$, as shown in Fig. 3 by the solid line, but has additional temperature dependence. The additional term takes into account the resistivity due to electron-magnon scattering. In general, the resistivity due to electrons scattering from an arbitrary type of boson excitation (magnon or phonon) can be written as[24]

$$\rho_B=\frac{m\pi N(0)}{ne^2}\int_0^{2k_F}\frac{k^3}{k_F^2}dk\int\frac{d\Omega_{\vec{k}}}{4\pi}|g_{\vec{k}}|^2\frac{\frac{\hbar\omega_{\vec{k}}}{k_BT}}{4\sinh^2\frac{\hbar\omega_{\vec{k}}}{2k_BT}}. \quad (2)$$

Here, $n=k_F^3/3\pi^2$ is the number density of the charge carriers, $N(0)=mk_F/2\pi^2\hbar^2$ is the density of states per spin at the Fermi level, $2k_F$ represents the maximum wave-vector transfer, $g_{\vec{k}}$ is the electron-boson coupling, k_B is the Boltzmann constant and $\hbar\omega_{\vec{k}}$ is the boson energy for a given wave vector $\vec{k}$. We shall apply Eq. (2) to either the ferromagnetic or antiferromagnetic case, as derived in the appendices.

The total resistivity below the transition temperature can be written as

$$\rho^{FM}=BT\Delta\left(1+\frac{2T}{\Delta}\right)e^{-\Delta/T},$$

or

$$\rho^{AFM}\approx C\Delta^5e^{-\Delta/T}\left\{\frac{1}{5}\left(\frac{T}{\Delta}\right)^5+\left(\frac{T}{\Delta}\right)^4+\frac{5}{3}\left(\frac{T}{\Delta}\right)^3\right\}. \quad (3)$$

In the gapless limit $\Delta\to0$, we obtain $\rho\sim T^2$ and $\sim T^5$ from Eq. (3) for the ferromagnetic (FM) case and the antiferromagnetic (AFM) case, respectively, as discussed in Ref. 22. In practice, to apply Eq. (3) to our data, we fit the first two terms of Eq. (3) at a very low temperature (0.7 K to ~3 K) to obtain ρ_0 and A, as shown in the inset of Fig. 3. These parameters are then fixed and the parameters in Eq. (3) are obtained by a higher temperature fit up to ~8 K for both FM and AFM cases. We find the parameters corresponding to this fit are $\rho_0=(0.17\pm0.03)$ $\mu\Omega$ cm, $A=(0.08\pm0.01)$ $\mu\Omega$ cm K^{-2}; $B=(3.3\pm0.2)$ $\mu\Omega$ cm K^{-2}, $\Delta=(24.4\pm0.5)$ K (FM) and $C=(1.30\pm0.02)\times10^{-3}$ $\mu\Omega$ cm K^{-5}, $\Delta=(10.5\pm0.5)$ K (AFM). Although small, there is a significant difference between these two fits at lower temperatures and fields. By applying this fitting procedure to the field-dependent resistivity for $H\perp c$ axis, we

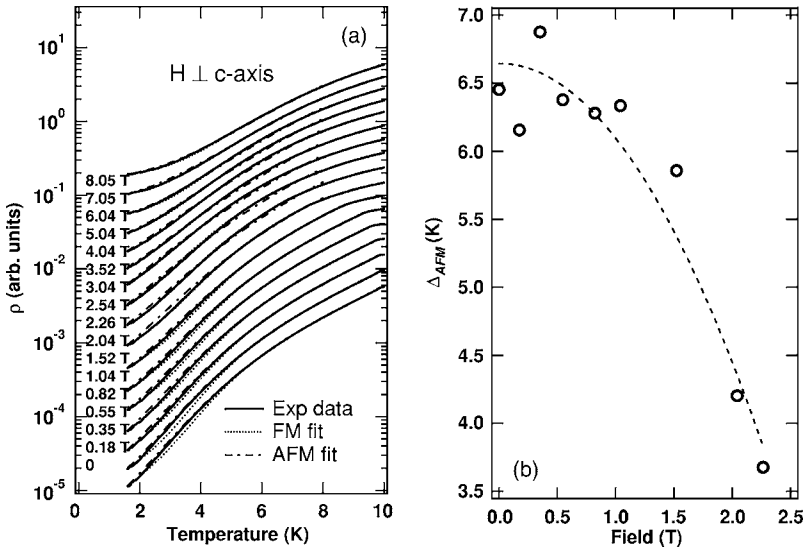

FIG. 4. (a) The in-plane dc resistivity (curves offset for clarity) vs temperature for different fields ($H\perp c$ axis). The dotted and dashed-dotted lines indicate fits to FM and AFM, respectively. (b) The field dependence of AFM gap energy Δ_{AFM}. The dashed line is a guide to the eye.

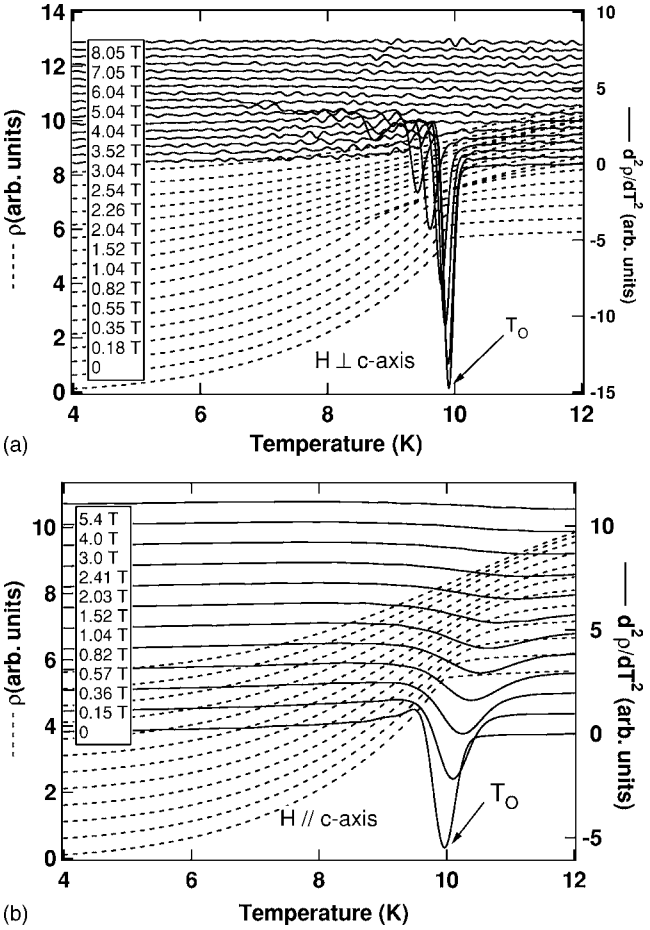

FIG. 5. The in-plane dc resistivity (curves offset for clarity) vs temperature for different fields (top: $H \perp c$ axis; bottom: $H \| c$ axis). The dashed and solid lines indicate the experimental data and $d^2\rho/dT^2$, respectively. The arrow indicates the transition temperature T_O.

are able to see more clearly these differences, as shown in Fig. 4(a), where in the low field limit, the AFM description gives the best fit. This suggests antiferromagnetic ordering in the basal plane below T_O. At higher fields, the spins will align parallel to the external magnetic field, favoring ferromagnetic order. We have determined the effect of the magnetic field on the AFM energy gap Δ_{AFM}, as shown in Fig. 4(b), and find the magnetic field reduces the gap energy. This is not surprising because in the antiferromagnetic case, the gap will be modified[25] by $\Delta_H = \Delta - \mu_{eff} H_{eff}$, where μ_{eff} is the effective magnetic moment and $H_{eff} = H - H_M$ which is the sum of the applied magnetic field and molecular field H_M produced by the other moments. In contrast, for $H \| c$ axis both FM and AFM fits work well at low fields, but only the FM fit is adequate at higher fields. Thus, this suggests that the ferromagnetic ordering is along the c axis.

The effect of magnetic field on the ordering temperature T_O is shown, for both magnetic fields applied parallel and perpendicular to the c axis in Fig. 5. We use the minimum of the second derivative of the resistivity with respect to the temperature $[(d/dT)(d^2\rho/dT^2) = 0]$ as the criterion for the ordering temperature, which is indicated by an arrow in Fig. 5. We observed that the ordering temperatures have different

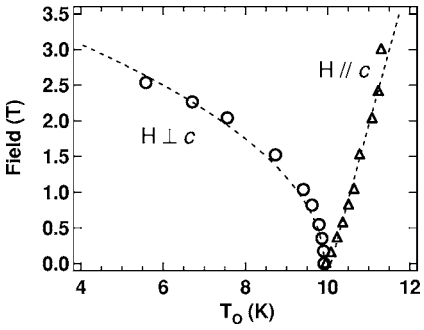

FIG. 6. Magnetic phase diagram of $CeAgSb_2$ based on the MR data. The open circles and triangles are the transition field for $H \perp c$ axis and $H \| c$ axis, respectively, obtained from Fig. 5. The dashed lines are guides to the eye.

behavior depending on the direction of the applied magnetic field. For $H \perp c$ axis, T_O decreases as the external field increases, following antiferromagnetic behavior. In contrast, for $H \| c$ axis, T_O increases as the external field increases, which is consistent with the ferromagnetic order. From this analysis, we attempt to construct the magnetic phase diagram of this compound, as shown in Fig. 6. This result is similar to that obtained in Ref. 7, which is estimated from the magnetization and the thermal expansion measurements. We will see later that this magnetic phase diagram is consistent with the CEF analysis.

The magnetoresistance (MR) of this compound, defined as $\{\rho(H,T) - \rho(0,T)\}/\rho(0,T)$, for the two different orientations is shown in Fig. 7. The MR changes sign below a characteristic temperature T_m from negative to positive.

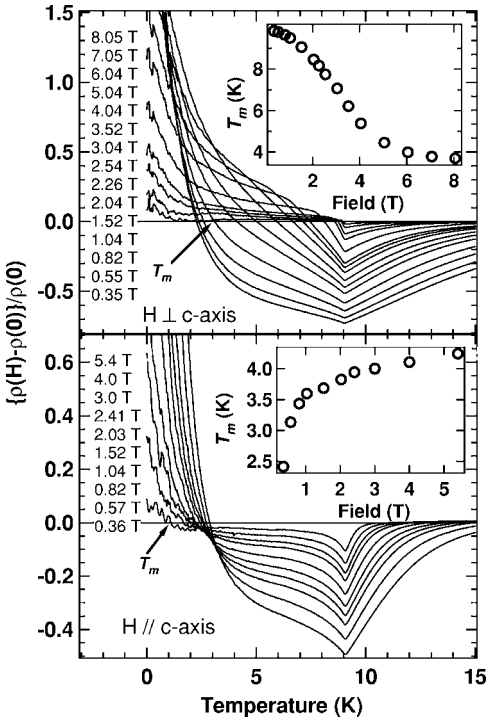

FIG. 7. The magnetoresistance of $CeAgSb_2$ as a function of temperature for top: $H \perp c$ axis and bottom: $H \| c$ axis. Insets: the field dependence of the characteristic T_m at which $[\rho(H) - \rho(0)] = 0$.

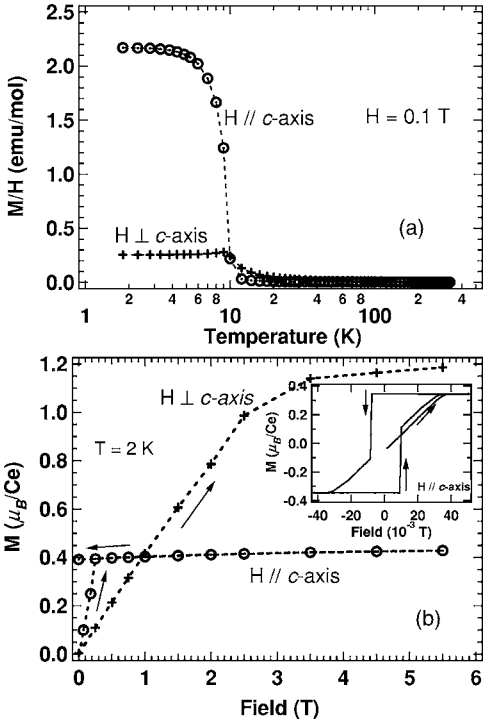

FIG. 8. (a) Temperature dependence of the susceptibility of $CeAgSb_2$ both for field applied parallel and perpendicular to the c axis, at $H=0.1$ T. (b) Field dependence of magnetization for two different field directions at $T=2$ K. The dashed lines are guides to the eye. Inset: the magnetization at low field for $H\|c$ axis.

Here, T_m also decreases or increases depending on the direction of the applied field (see the insets in Fig. 7). The anisotropy of T_m also suggests that the system has different magnetic ordering for the different field directions. In both cases, T_m saturates at a certain field. The behavior of the MR above and below T_m can be explained as follows. Above T_m, the negative character of the MR is due to the reduction in electron-spin scattering, since as the magnetic field increases, the effective field suppresses the fluctuations of the localized spins, leading to an increase in the conductivity. Below T_m, when the magnetic field increases, the gap energy Δ decreases and more magnons will be in the excited state, which causes more electron-magnon scattering, increasing the resistivity.

B. Magnetic properties

The magnetization measurement of $CeAgSb_2$ exhibits magnetic ordering below $T_O \sim 9.8$ K as shown in Fig. 8(a), where we note that below T_O the magnetization is anisotropic with respect to field direction. The temperature dependence of the magnetization under 0.1 T for the field perpendicular to the c axis shows a cusp around T_O, which is usually found in an antiferromagnetic transition. We have used the Curie-Weiss law to fit the susceptibility data at high temperature. For $H\|c$ the effective magnetic moment and Curie temperature are $\mu_{eff}=2.51\mu_B$/Ce and $\Theta_C=-63.9$ K. For $H\perp c$, $\mu_{eff}=2.48\mu_B$/Ce and $\Theta_C=5.05$ K. Both effective magnetic moments are close to the theoretical value of $2.54\mu_B$/Ce for Ce^{3+} ($S=\frac{1}{2}$; $L=3$; $J=\frac{5}{2}$). The magnetization isotherm for $H\perp c$ data at $T=2$ K, as shown in Fig. 8(b), increases almost linearly below 3.5 T and then remains nearly constant at high field with a saturated moment $\sim 1.2\mu_B$/Ce. No hysteresis is found, suggesting this compound is antiferromagnetically ordered for $H\perp c$. In contrast, for $H\|c$, a saturation magnetic moment of $\sim 0.4\mu_B$/Ce is found at a low field (~ 0.04 T). Hysteresis with a remnant magnetic field ~ -0.01 T is observed, as shown in the inset of Fig. 8(b), indicating ferromagnetic order.

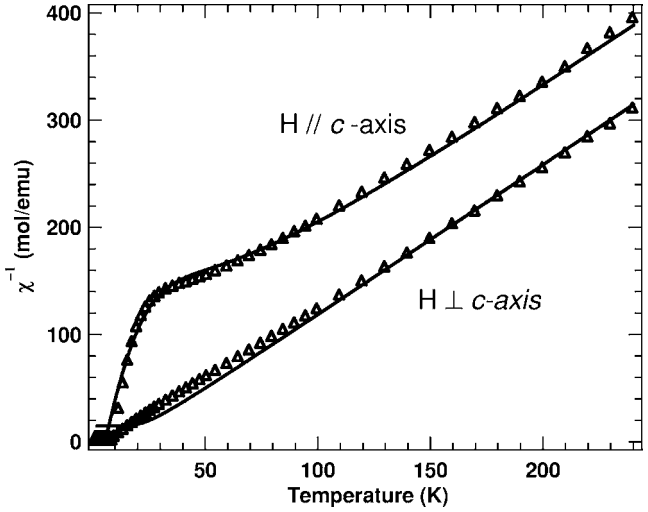

FIG. 9. The temperature dependence of the inverse magnetic susceptibility of $CeAgSb_2$ for two field directions at $H=0.1$ T. Triangles indicate experimental data and the solid lines are the calculated curves based on Eq. (8).

The Kondo temperature for a single-ion and nonmagnetic order can be estimated by using[26,27]

$$T_K = \frac{(\nu-1)\pi RW}{6\gamma}, \tag{4}$$

where $\nu=2J+1=2$, W is the Wilson number$=1.289$, R is the universal gas constant$=8.314$ J mol^{-1} K^{-1} and γ is the Sommerfeld coefficient ~ 244 mJ mol^{-1} K^{-2}. We estimate the Sommerfeld coefficient by using $[C(T)]/T=\gamma+aT^2$, where C is the specific heat, in the temperature range between 20 K and 12 K, which is above the ordering temperature. The Kondo temperature obtained from Eq. (4) is $T_K=23$ K, which is similar to $T_{max}\sim 15$ K (see Fig. 2). This comes from the doublet ground state in the CEF analysis and the low-temperature estimate for T_K.

In contrast to the above approach, if we consider multiplet states $\left(J=\frac{5}{2}\right)$ from the CEF analysis then we obtain a high-temperature estimate for T_K of ~ 65 K, which is derived from the inverse susceptibility data (see Fig. 9).[28] This high-temperature T_K is comparable to the inelastic neutron scattering (T_K is between 60 and 80 K)[13] and μSR ($T_K \sim 60$ K.[16]

1. Crystalline electric field theory

We next discuss the magnetic properties based on the CEF theory. The total Hamiltonian is given as follows,

TABLE I. CEF parameters, energy level, molecular field parameters λ and corresponding wave functions for $CeAgSb_2$.

CEF Parameters	B_2^0=6.60 K		B_4^0=−0.09 K		B_4^4=1.14 K	
	$\lambda_{\parallel c\text{-axis}}$=47.9 mol/emu		$\lambda_{\perp c\text{-axis}}$=−14.8 mol/emu			
Energy (K)	$\|+\frac{5}{2}\rangle$	$\|+\frac{3}{2}\rangle$	$\|+\frac{1}{2}\rangle$	$\|-\frac{1}{2}\rangle$	$\|-\frac{3}{2}\rangle$	$\|-\frac{5}{2}\rangle$
137	0.919	0	0	0	−0.394	0
137	0	0.394	0	0	0	−0.919
53	0	−0.919	0	0	0	−0.394
53	0.394	0	0	0	0.919	0
0	0	0	1	0	0	0
0	0	0	0	1	0	0

$$\mathcal{H} = \mathcal{H}_{CEF} - g_j \mu_B J_i (H_i + \lambda_i M_i), \tag{5}$$

where g_j is the Lande g factor ($\frac{6}{7}$ for Ce^{3+}), μ_B is the Bohr magnetron, J_i ($i=x$, y, and z) is the component of angular momentum, M_i is the magnetization, and $\mathcal{H}_{CEF}$ is the CEF Hamiltonian. The second and third terms of the Hamiltonian are the contributions from the Zeeman effect and the molecular field. The CEF Hamiltonian of this system, which has a tetragonal symmetry, can be written as

$$\mathcal{H}_{CEF} = B_2^0 O_2^0 + B_4^0 O_4^0 + B_4^4 O_4^4, \tag{6}$$

where B_k^q and O_k^q are the CEF parameters and the Stevens operators, respectively.[29,30] The $Ce^{3+}(4f^1)$ ion has an odd number of electrons in the $4f$ shell and qualifies as a Kramers ion with a doublet ground state. The CEF effect splits the $4f$ level into three doublets with excitation energy Δ_1 and Δ_2 from the ground state to the first and second excited states, respectively. The temperature dependence of the susceptibility based on CEF model can be expressed as

$$\chi_{CEF}^i = N(g_j\mu_B)^2 \times \frac{1}{Z}\left(\sum_{m\neq n} |\langle m|J_i|n\rangle|^2 \times \frac{1-e^{-\Delta_{mn}/k_BT}}{\Delta_{mn}} \times e^{-E_n/k_BT} + \frac{1}{k_BT}\sum_n |\langle n|J_i|n\rangle|^2 \times e^{-E_n/k_BT} \right). \tag{7}$$

Here, index i indicates the axis(x, y, or z axis), N is the number of ions, E_n is the energy at state n, Z is a partition function, and $\Delta_{mn}=E_n-E_m$. The total magnetic susceptibility including the molecular field contribution is given by

$$\chi_i^{-1} = (\chi_{CEF}^i)^{-1} - \lambda_i. \tag{8}$$

Figure 9 shows the inverse magnetic susceptibility as a function of temperature for different field directions. The calculated susceptibility for $H\|c$ agrees well with the experimental results, but for $H\perp c$ there is a small deviation. We obtain the CEF parameters (see Table I) by fitting the data using Eq. (8). In this model, we find that the wave functions of the ground state are $|\pm\frac{1}{2}\rangle$ with a saturation moment of $0.4\mu_B$/Ce along the c axis, which is in agreement with the predicted saturation moment of the ground state, $g_j\mu_B J_z = 0.43\mu_B$/Ce. The energy levels obtained by this fitting are consistent with previous results.[7] Also, the excitation energies of ~60 K and ~145 K are consistent with neutron-scattering experiments.[18] The molecular field parameter λ is proportional to the exchange interaction between nearest neighbors and is negative (positive) for the antiferromagnetic (ferromagnetic) case. In Table I, we find λ is negative for the $H\perp c$ and positive for $H\|c$, which is consistent with the magnetic phase diagram obtained from resistivity measurement (see Fig. 6).

C. Shubnikov-de Haas oscillations

The Fermi surface of $CeAgSb_2$ has been systematically studied by Inada *et al.*[5] by angular dependent dHvA measurements, which involve the determination of the oscillatory magnetization vs inverse field. The large cylindrical corrugated Fermi surfaces with large cyclotron masses ($20-30m_e$) were obtained in Ref. 5. Theoretically, the modified $4f$-localized electron band calculation was proposed to explain some of the dHvA frequencies observed in the experiment. We have studied the temperature dependence of the SdH in $CeAgSb_2$ in high fields (to 32 T) to helium temperatures, and in lower fields (18 T) to 80 mK vs magnetic field direction. In the SdH measurement, the oscillatory magnetoresistance, upon which may be imposed a background magnetoresistance, is measured. In a previous study,[21] the SdH of $CeAgSb_2$ under pressure (1.2 kbar) for $H\|c$ showed a single SdH frequency of 25 T. As in Ref. 19, we find the predominant frequency to be ~25 T, as shown in Fig. 10(a), and in the high field (above 25 T), we observe another frequency (~300 T) below 2 K. We note the main oscillation frequency is significantly less than the lowest frequency (~40 T) observed previously in the dHvA measurements.[5] We find that the amplitude of the 25 T oscillation is highly dependent on field orientation, where a tilt of only 7° away from the c axis causes a significant decrease in amplitude [Fig. 10(b)]. Figure 11 shows the effective cyclotron mass (M_c) for the 25 T orbit, which is $\sim 3m_e$, extracted from the Lifshitz-Kosevich formula,[31] where we note that the effective mass, unlike the SdH amplitude, is not sensitive to the small change in angle. The cyclotron mass obtained in the previous dHvA measurement[5] is only $0.85m_e$ for the 41 T

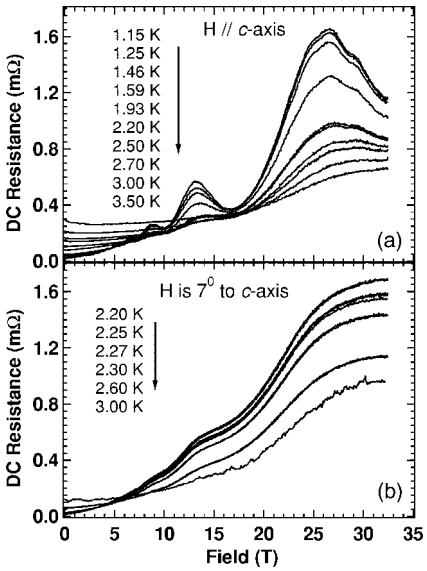

FIG. 10. Temperature dependence of Shubnikov-de Haas oscillations of $CeAgSb_2$ up to 32 T for two different angles. The dominant frequency is ~25 T and another frequency (~300 T) is visible above 25 T and below 1.5 K.

frequency. The Dingle temperature, which is related to the scattering rate, is 0.37 K and 0.66 K for the fields parallel to the c axis and 7° from the c axis, respectively.

The angular dependence of the SdH signal was studied more systematically at low temperature (~80 mK) to 18 T, as shown in Fig. 12(a). We observe two different frequencies (~25 T and ~600 T) depending on the angle between the field and the c axis, as shown in Fig. 12(b). In this sample, we did not detect the 300 T frequency. The inset of Fig. 12(b) shows the amplitude of the 25 T oscillation for different angles. The amplitude of the oscillation has a maximum around 95°, which is 5° off from the c axis, and very dramatically decreases away from 95°. The SdH oscillations below 80° or above 115° are very weak, and no SdH oscillations associated with the 25 T frequency are observable outside this range. Both measurements indicate that the SdH amplitudes are very sensitive to magnetic field direction.

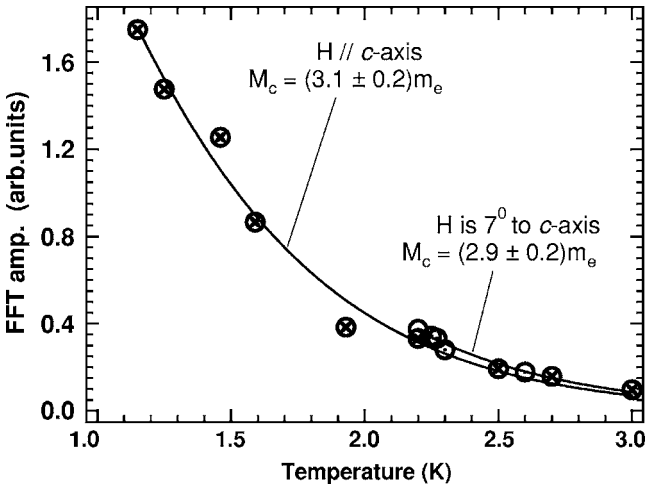

FIG. 11. The fast Fourier transform amplitude of the 25 T SdH oscillation in $CeAgSb_2$ vs temperature for two different angles. The solid lines are fits to the Lifshitz-Kosevich effective mass expression.

The band calculation[5] suggests that the Fermi surface of $CeAgSb_2$ is similar to those of $LaAgSb_2$. The dHvA experiments indicate that the best model is one where the band structure is modified by the $4f$-localized electron system.[5] This model has been successfully used to explain the topology of Fermi surfaces in Ce compounds with magnetic order, such as $CeAl_2$ and CeB_6.[32,33] However, this model cannot describe all the frequencies observed in both SdH and dHvA measurements in $CeAgSb_2$. Moreover, the decrease in the SdH frequency away from $H\|c$ is inconsistent with a simple two-dimensional cylindrical Fermi surface directed along the c axis. Nevertheless, if the main Fermi surface cylinders are corrugated, as the tilt angle increases, the cyclotron mass and frequency will decrease.[34] Furthermore, the amplitude of oscillation might also be strongly affected by changes in the lens orbit topology as the angle moves away from 90°. The main Fermi surface, which has frequency of 11.2 kT, was not observed in this measurement. This might be due to the relatively large effective cyclotron mass or to some other at present unknown fundamental difference between dHvA (a thermodynamic probe) and SdH (a transport probe) measurements in the present case.

IV. CONCLUSION

We have performed magnetic and electrical transport measurements on single crystalline $CeAgSb_2$ to further explore its magnetic ground state. At the zero field, the magnetic transition, based on transport theory which includes magnon scattering, indicates that antiferromagnetic order appears below $T_O \sim 9.8$ K. The MR data, again compared with the magnon model, shows that at the finite field antiferromagnetic order is present for in-plane field, and the ferromagnetic order for the field along the c axis. One type of magnetic ground state that would lend itself to this anisotropy is a canted antiferromagnetic configuration in the basal plane. However, Araki *et al.*[18] concluded that the magnetic ground state in the polycrystalline $CeAgSb_2$ from neutron scattering is a simple ferromagnetic order. It would be very useful to test this contradiction by doing a neutron-scattering experiment on a single crystal to determine in detail the spin alignments.

The magnetic H-T phase diagram we obtain from MR data is consistent with that found in previous magnetization and thermal expansion measurements.[7] A fit of the magnon model to the data yields a field-dependent magnon energy gap, which is found to decrease with the increasing field. Complementary to the field-dependent magnon gap is the observation that the MR changes sign at a temperature T_m below T_O. T_m depends on the magnetic field and its direction, and we present arguments to describe this effect.

Previous estimates of the T_K have varied widely. From the doublet ground state $\left(J=\frac{1}{2}\right)$ and multiplet states $\left(J=\frac{5}{2}\right)$, we obtain both low-temperature and high-temperature estimates for T_K of ~23 K and ~65 K, respectively. The high-temperature T_K is similar to those obtained from preliminary

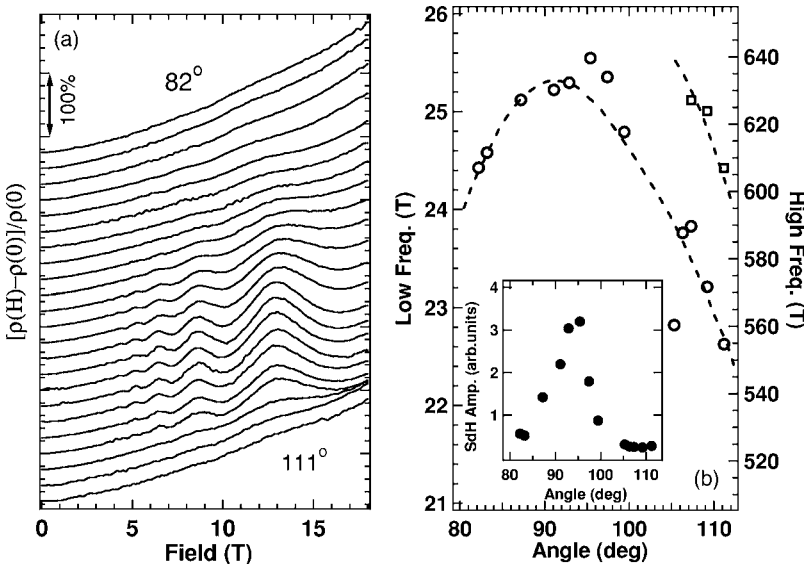

FIG. 12. (a) The SdH oscillations of $CeAgSb_2$ for different angles at $T \sim 80$ mK up to 18 T. The 600 T frequency can be detected in several curves above 15 T (i.e., 109°, 111°) by subtracting the MR background. (b) SdH frequency vs angle, dashed line is a guide to the eye. Inset: the amplitude of the oscillation vs angle.

inelastic-neutron-scattering and μSR measurements.

Remaining aspects of the $CeAgSb_2$ system that will require further investigation are the SdH results. We find that, in agreement with a previous preliminary study, a small (25 T) orbit dominates the SdH signal, indicating significant differences between the SdH and previous dHvA results where no frequency below 40 T is observed. Moreover, unlike the dHvA, there seems to be a very strong attenuation of the SdH signal with field direction. Although SdH is sensitive to Stark-interference-type orbits that have no thermodynamic weight, it is not clear why the 25 T is so evident, or if it does indeed arise from lenslike orbits from intersecting Fermi surface sections at the zone boundaries. It is also possible that the magnetic ground state may influence the electronic structure or the carrier mean-free path in some unknown manner. Further high-field SdH and dHvA comparative measurements are planned to explore these questions.

ACKNOWLEDGMENTS

This research was sponsored by the National Nuclear Security Administration under the Stewardship Science Academic Alliances Program through DOE Research Grant No. DE-FG03-03NA00066, NSF Grant No. DMR-0449569, and the NHMFL is supported by a contractual agreement between the NSF and the state of Florida. We would like to thank P. Schlottmann for fruitful discussions.

APPENDIX A: FERROMAGNETIC CASE

In the case of an anisotropic ferromagnetic (FM) material, there is a gap Δ in the magnon spectrum, and the energy dispersion relation of the magnon[24] can be expressed by $\hbar\omega_{\vec{k}} = \Delta + C_0 k^2$, where C_0 is the spin-wave stiffness. The electron-magnon coupling $|g_{\vec{k}}|^2$ for ferromagnetic system is independent[35] of $\vec{k}$. In the limit of $\hbar\omega_{\vec{k}}/2k_BT \gg 1$, the leading term of electron-magnon resistivity in the anisotropic ferromagnetic material ρ^{FM} can be written as

$$\rho^{FM}(T) = BT\Delta\left(1 + \frac{2T}{\Delta}\right)e^{-\Delta/T}, \tag{A1}$$

where B is a constant related to the spin disorder.

APPENDIX B: ANTIFERROMAGNETIC CASE

In the case of antiferromagnetic (AFM) system, the electron-magnon coupling[24] $|g_{\vec{k}}|^2 \propto k$ and the energy dispersion relation[36] is $\hbar\omega_{\vec{k}} = \sqrt{\Delta^2 + Dk^2}$. By using the information given above, we obtain

$$\rho^{AFM}(T) = \frac{C}{T}\int_0^\infty \frac{k^4\sqrt{\Delta^2 + Dk^2}}{\sinh^2(\sqrt{\Delta^2 + Dk^2}/2T)}dk, \tag{B1}$$

where C is a constant. Using the change of variable, $y = \sqrt{\Delta^2 + Dk^2}/2T$, one can approximate $\sinh^2 y \approx e^{2y}$ in the small temperature limit $T \ll \Delta$, and find

$$\rho^{AFM}(T) = CT^5\int_{y_0}^\infty y^2(y^2 - y_0^2)^{3/2}e^{-2y}dy, \tag{B2}$$

where $y_0 = \Delta/2T$. This integral can be easily calculated if we use another change of variable $y = y_0\cosh(x)$, so that

$$\rho^{AFM} = CT^5 y_0^5 e^{-2y_0}\int_0^\infty (\cosh^2 x \sinh^3 x \times e^{(-2y_0\cosh x + 2y_0)})dx. \tag{B3}$$

The integrand of Eq. (B3) is asymptotic to zero above a certain x, so that it can be simplified to $\cosh^2 x \sinh^3 x$, in which the function $e^{-2y_0\cosh x + 2y_0}$ acts as a cutoff in the integral. The limit of the integral then is from 0 to x_c, where x_c is the solution of $-2y_0\cosh x_c + 2y_0 = -1$, and Eq. (B3) becomes

$$\rho^{AFM}(T) \approx CT^5 y_0^5 e^{-2y_0}\int_0^{x_c} \cosh^2 x \sinh^2 x dx. \tag{B4}$$

Thus, the leading term of the resistivity in the antiferromagnetic case is given by

$$\rho^{AFM} \approx C\Delta^5 e^{-\Delta/T}\left\{\frac{1}{5}\left(\frac{T}{\Delta}\right)^5 + \left(\frac{T}{\Delta}\right)^4 + \frac{5}{3}\left(\frac{T}{\Delta}\right)^3\right\}. \tag{B5}$$

[1] H. B. Radousky, *Magnetism in Heavy Fermion Systems* (World Scientific, Singapore, 2000).
[2] G. R. Stewart, Rev. Mod. Phys. **56**, 755 (1984).
[3] K. D. Myers, S. L. Bud'ko, I. R. Fisher, Z. Islam, H. Kleinke, A. H. Lacerda, and P. C. Canfield, J. Magn. Magn. Mater. **205**, 27 (1999).
[4] F. Steglich, J. Aarts, C. D. Bredl, W. Lieke, D. Meschede, W. Franz, and H. Schfer, Phys. Rev. Lett. **43**, 1892 (1979).
[5] Y. Inada *et al.*, Philos. Mag. B **82**, 1867 (2002).
[6] Y. Muro, N. Takeda, and M. Ishikawa, J. Alloys Compd. **257**, 23 (1997).
[7] T. Takeuchi *et al.*, Phys. Rev. B **67**, 064403 (2003).
[8] K. Sengupta *et al.*, Phys. Rev. B **70**, 064406 (2004).
[9] E. Sampathkumaran *et al.*, Physica B **359–361**, 108 (2005).
[10] P. M. Levy and S. Zhang, Phys. Rev. Lett. **62**, 78 (1989).
[11] O. Sologub, H. Noël, A. Leithe-Jasper, P. Rogl, and O. I. Bodak, J. Solid State Chem. **115**, 441 (1995).
[12] M. Brylak, M. H. Möller, and W. Jeitschko, J. Solid State Chem. **115**, 305 (1995).
[13] M. J. Thornton, J. G. M. Armitage, G. J. Tomka, P. C. Riedi, R. H. Mitchell, M. Houshiar, D. T. Adroja, B. D. Rainford, and D. Fort, J. Phys.: Condens. Matter **10**, 9485 (1998).
[14] M. Houshiar, D. T. Adroja, and B. D. Rainford, J. Magn. Magn. Mater. **140–141**, 1231 (1995).
[15] A. Thamizhavel *et al.* Phys. Rev. B **68**, 054427 (2003).
[16] J. A. Dann, A. D. Hillier, J. G. M. Armitage, and R. Cywinski, Physica B **289–290**, 38 (2000).
[17] G. André, F. Boure, M. Kolenda, B. Lesniewska, A. Oles, and A. Szytula, Physica B **292**, 176 (2000).
[18] S. Araki, N. Metoki, A. Galatanu, E. Yamamoto, A. Thamizhavel, and Y. Onuki, Phys. Rev. B **68**, 024408 (2003).
[19] K. D. Schotte and U. Schotte, Phys. Lett. A **55**, 38 (1975).
[20] V. A. Sidorov, E. D. Bauer, N. A. Frederick, J. R. Jeffries, S. Nakatsuji, N. O. Moreno, J. D. Thompson, M. B. Maple, and Z. Fisk, Phys. Rev. B **67**, 224419 (2003).
[21] K. D. Myers, S. L. Bud'ko, V. P. Antropov, B. N. Harmon, P. C. Canfield, and A. H. Lacerda, Phys. Rev. B **60**, 13371 (1999).
[22] J. S. Schilling, Phys. Rev. B **33**, 1667 (1986).
[23] A. P. Pikul, D. Kaczorowski, T. Plackowski, A. Czopnik, H. Michor, E. Bauer, G. Hilscher, P. Rogl, and Y. Grin, Phys. Rev. B **67**, 224417 (2003).
[24] N. H. Andersen and H. Smith, Phys. Rev. B **19**, 384 (1979).
[25] S. A. M. Mentink, T. E. Mason, S. Sullow, G. J. Nieuwenhuys, A. A. Menovsky, J. A. Mydosh, and J. A. A. J. Perenboom, Phys. Rev. B **53**, R6014 (1996).
[26] V. T. Rajan, Phys. Rev. Lett. **51**, 308 (1983).
[27] N. Andrei and J. H. Lowenstein, Phys. Rev. Lett. **46**, 356 (1981).
[28] G. Grüner and A. Zawadowski, *Progress in Low Temperature Physics* (Amsterdam: North Holland, 1978), Vol. VII B.
[29] K. W. H. Stevens, Proc. Phys. Soc., London, Sect. A **65**, 209 (1952).
[30] M. T. Hutchings, in *Solid State Physics: Advances in Research and Applications*, edited by T. Seitz (Academic, New York, 1965), Vol. 16.
[31] J. Wosnitza, *Fermi Surfaces of Low-Dimensional Organic Metals and Superconductors* (Springer, New York, 1996).
[32] M. Springford and P. H. P. Reinders, J. Magn. Magn. Mater. **76–77**, 11 (1988).
[33] Y. Onuki, T. Komatsubara, P. H. P. Reinders, and M. Springford, J. Phys. Soc. Jpn. **58**, 3698 (1989).
[34] A. B. Henriques, V. N. Morgoon, P. L. de Souza, V. Bindilatti, N. F. Oliveira, Jr., and S. M. Shibli, Phys. Rev. B **49**, 11248 (1994).
[35] A. Sumiyama, Y. Oda, H. Nagano, Y. Onuki, K. Shibutani, and T. Komatsubara, J. Phys. Soc. Jpn. **55**, 1294 (1986).
[36] M. B. Fontes, J. C. Trochez, B. Giordanengo, S. L. Bud'ko, D. R. Sanchez, E. M. Baggio-Saitovitch, and M. A. Continentino, Phys. Rev. B **60**, 6781 (1999).